Novel back-end-of-line compatible method for integration of inductances with magnetic core on silicon

Malte Paesler, Thomas Lisec, and Holger Kapels
Malte.Paesler@isit.fraunhofer.de
Fraunhofer Institute for Silicon Technology ISIT, Fraunhoferstr. 1, 25524 Itzehoe, Germany

Abstract

In high frequency applications like power supplies, the integration of active and passive components on a single chip is necessary to increase the power density. A novel approach for the integration of micro-inductances with a magnetic core on silicon substrates is presented. This paper shows development, processing and investigation of different samples, having a magnetic core of 3.4 mm x 1 mm x 0.6 mm in size. At 20 MHz inductances of 150 nH are reached, whereas the resistance is about 0.66 Ω. The fabrication technique is based on the agglomeration of micron-sized magnetic powder by atomic layer deposition (ALD). The process is fully back-end-of-line (BEOL) compatible and offers a wide range of magnetic materials, which can be integrated on the substrate in any desired geometry of the core. This enables a lot of possibilities for the integration and design of inductors.

1 Introduction

Smaller packages and therefore higher power densities for power supplies are important developments in the future for technologies like IoT, smart homes, smartphones etc. Active power devices like silicon carbide and gallium nitride field effect transistors enable switching frequencies in megahertz range leading to inductances below 200 nH for typical dc-dc converters [1], [2]. Thus, the approach for inductor design combined with MEMS fabrication processes seems to be an important aspect for integrating a power supply in a package (PwrSiP) [3] or a power supply on a chip (PwrSoC) [4]. In [5, 6, 7] different inductor designs and fabrication processes on silicon were investigated, where the windings are built mainly on the surface like spiral inductors [8]. Whereas, 3D air-core inductors were developed using through-silicon vias (TSV) in [9],[10]. These 3D inductors have already a better inductance density compared to spiral inductors, but without a magnetic core the inductance density is still quite low.

This paper presents an approach combining both ideas, a 3D-inductor and a magnetic core to improve the inductance density. Thinking about integration and solutions for a power supply in a package, it might be interesting to build the inductor and transistor on the same substrate, coming along with benefits like low parasitics and better thermal behavior.

In this paper, magnetic cores based on micron-sized, soft magnetic powder on silicon substrate are used, applying a method of powder agglomeration described in [11]. Due to the dielectric layer between all particles from the ALD process, the contact surface between each particle is quite small, which suppresses eddy currents and good characteristics are obtained even at high frequencies. Several magnetic powders provided from different suppliers with particle sizes between 1 µm and 100 µm were characterized regarding their magnetic and electrical behavior and proved their compatibility to the applied fabrication method. In addition, mixtures of powders were investigated. A copper wire is hand-wound around the magnetic core to obtain an inductor. Measurements on a vibrating sample magnetometer (VSM) and on an impedance analyzer show big differences between the investigated magnetic powder based cores. Beside the measurements, finite-element-method (FEM) simulations are done for validation and parameter tuning of the magnetic powder for future designs. Following to these investigations, inductors based on powder based cores with TSVs instead of hand-wound wires will be fabricated in optimized design.

The paper is divided as follows. In section 2, the fabrication method of magnetic powder based cores is described and an approach for further fabrication ideas with TSVs is explained. The measurement results and characterization of these samples are discussed in section 3. First, microscope images show the structure and proof the fabrication method. Besides, electrical and magnetic measurements are presented to compare several different samples. Section 4 introduces the FEM simulations and shows comparable results to the measured curves of the previous section.

2 Magnetic core fabrication method

Magnetic cores are realized on silicon substrates, using a novel fabrication technique, which is based on the agglomeration of micron-sized particles by atomic layer deposition. The basic principle is illustrated in Figure 1 on the left. At mold pattern created within a substrate is filled with loose micron-sized particles. Then the substrate is subjected to an ALD process. With optimized process conditions the loose particles in the molds are fixated to rigid

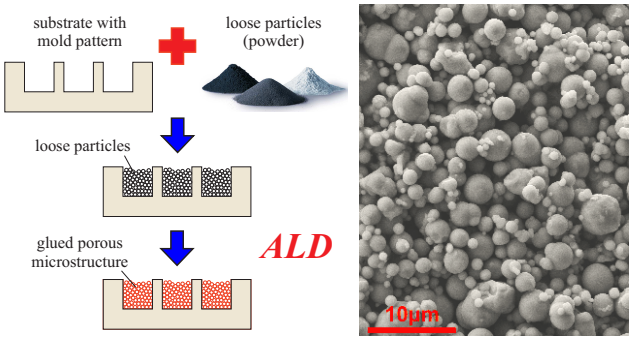

Figure 1 Fabrication method (left); SEM image of the bottom side of core P04, after removal of the surrounding silicon (right)

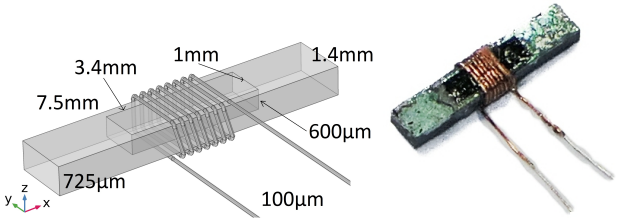

Figure 2 Sample geometry (left) and test samples (right)

porous 3D structures over the whole mold depth by an ALD layer with a thickness of only several tens of nanometers [11]. The novel technique has been utilized to create porous 3D structures for example from Al2O3, NdFeB and phosphor particles on 8 inch silicon substrates [11, 12, 13]. In Figure 1 on the right, the SEM image presents such a porous 3D structure agglomerated from iron particles. It was shown that substrates with embedded porous 3D structures are back-end-of-line (BEOL) compatible and can be post-processed in a cleanroom environment. For the piezoelectric vibrational harvester with integrated NdFeB micro magnet array as described in [14] after porous 3D structure integration three more mask layers as well as PECVD and various dry etching processes are applied to finalize the device. In [12] suitable conditioning procedures to regain the cleanroom compatibility of substrates with embedded porous 3D structures are described. Besides, the reproducibility of NdFeB-based porous 3D structures as well as their variation over a wafer is discussed.

Within the present work for the first time porous 3D structures were fabricated from soft magnetic powder. For that at first a pattern of 3400 µm long, 1000 µm wide and 600 µm deep cavities is created by deep reactive ion etching (DRIE) with an 8 inch silicon substrate. After resist removal and cleaning, the substrate is diced into pieces, about 40 mm x 40 mm in size. Now, the cavities on such a piece are manually filled with micron-sized magnetic particles of a particular material, using the doctor blade method. Carbonyl iron powder, alloy powder (QFeSi6.5) and MnZnP ferrite with particle sizes between 1 to 100 µm were tested. ALD of 75 nm Al2O3 at 200 °C is applied to agglomerate the loose particles within the cavities to rigid porous structures. By another dicing step, silicon chips as shown in Figure 3 on the right are cut from each piece. To

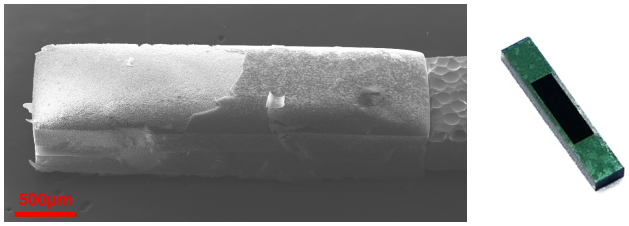

Figure 3 SEM image of the core P04, after partly removal of the surrounding silicon by etching in XeF2 gas phase (left); silicon chip with embedded magnetic powder-based core before the etching (right)

obtain inductors from those chips, 8 turns of 100 µm copper wire are manually wound around the central part with the embedded soft-magnetic core (Figure 2). Finally, the wire is fixed with instant adhesive. More sophisticated devices with optimized core and integrated windings will be designed and fabricated after the successful proof of the novel core material.

3 Measurements and characteristics

At first, several samples were investigated on a scanning electron microscope (SEM) to ensure a successful agglomeration of all particles in the cavity (section 3.1). Besides, all 19 processed samples were characterized without any wire on a vibrating sample magnetometer (LakeShore VSM 7400 system), investigating their permeability and magnetic saturation (section 3.2). For analysis of the inductance and resistance over a selected frequency range, measurements of the samples with 8 turns of 100 µm copper wire were taken on a high precision impedance analyzer (Agilent 4294A) (section 3.3).

3.1 Powder core microscopy

To confirm that the particles indeed were agglomerated down to the mold bottom on a few samples as shown on the left side of Figure 3, the surrounding silicon has been removed in XeF2 gas phase. The SEM image in Figure 3 presents one of this cores after release. On the right side, the core is enveloped by a passivisation stack including the Al2O3 ALD layer. On the left side, the passivisation was removed, so that the agglomerated particles are exposed. The SEM image in Figure 1 illustrates this particular area at higher magnification. A particle size between 2 µm and 8 µm as specified in the data sheet of this material can be confirmed. The Al2O3 ALD layer still cannot be seen, since it surrounds the particles perfectly like an exoskeleton. In [11], more details regarding the specifics of porous 3D structures including FIB cross-sections can be found.

3.2 Magnetic measurements

A magnetic field up to $H = 10^6 \mathrm{A/m}$ was applied to the samples, which were aligned with the long side parallel to the direction of the magnetic field, measuring the magnetic moment with four pick-up coils at room temperature. Especially, in the linear region, a high resolution was chosen.

Sample	B_{sat} [T]	μ_{max}	L* [nH]	R* [mΩ]	PO*
P01	1.93	6.0	133.9	543	no
P02	1.80	5.0	126.0	393	yes
P03	1.95	6.9	144.4	1401	no
P04	2.16	6.8	148.9	660	yes
P05	1.87	7.2	159.4	1233	no
P06	0.26	3.4	86.5	501	no
P07	0.39	4.6	112.5	669	no
P12	0.34	4.0	105.1	578	no
P19	0.86	5.2	130.5	518	yes
P20	0.41	5.1	111.9	498	no
P21	0.17	2.6	80.2	370	yes
P30	1.87	6.1	148.3	794	no
P31	1.71	5.4	136.0	538	yes
P32	1.61	4.7	126.8	446	yes
P33	1.59	4.7	116.3	410	no
P34	0.67	3.5	92.6	518	no
P35	1.99	7.3	160.6	983	(yes)
P36	1.86	4.1	158.9	1012	no
P37	0.72	6.0	101.7	452	no
Ref1			157.8	909	no
Ref2			163.4	868	yes
Ref3			150.8	2283	no

Table 1 Overview of measurement results (* at 20 MHz)

Different samples of the same magnetic powder core were measured and confirmed the results. In Figure 4 the results of four powder based cores and a sample without core are plotted. Because of the fabrication process, which leads to an oxid layer around each magnetic particle, all powders depict a narrow MH-curve with a small remanent magnetization. Table 1 summarizes the measurement results of each powder based core regarding the magnetic saturation flux density B_{sat} and the maximum permeability μ_{max}, which is in the range between 2.6 and 7.3.

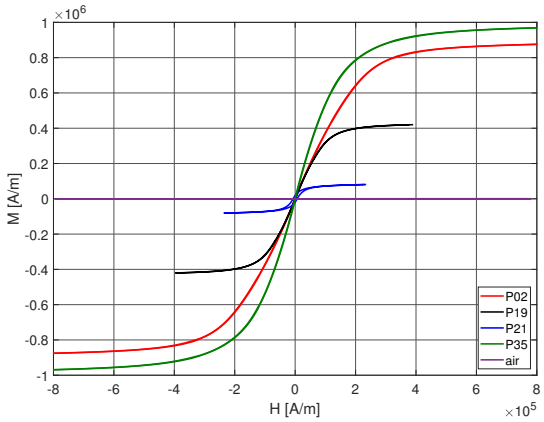

Figure 4 Measurement results (LakeShore VSM system)

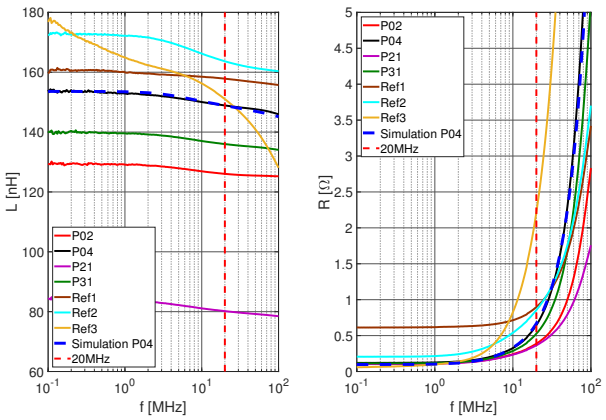

Figure 5 Measurement results of the Agilent 4294A: Inductance (left) and Resistance (right)

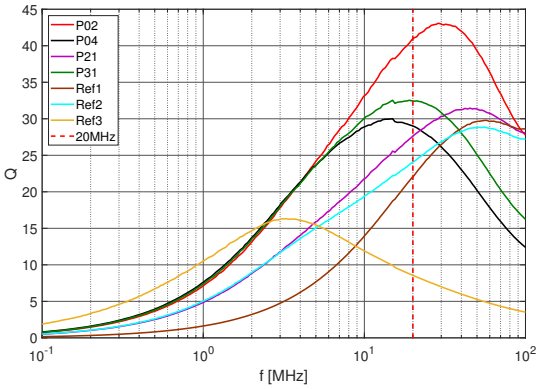

Figure 6 Measurement results of the Agilent 4294A: Quality factor

3.3 Electrical measurements

The high precision impedance analyzer was used in the range from from 100 kHz to 100 MHz, measuring the inductance and resistance of each sample. Beside the fabricated samples, three commercial available 150 nH inductors (Ref1, Ref2, Ref3) for high frequency applications from different manufacturers were measured for comparison. The plots are displayed in Figure 5 (inductance on the left and resistance on the right) and in Figure 6 (quality factor). The quality factor is given by

$$Q = \frac{L}{R} 2\pi f. \tag{1}$$

At 20 MHz, the inductances are between 80 nH and 165 nH, whereas the same geometry with an air-core reaches an inductance of 60 nH. Moreover, the resistance was measured between 0.37 Ω and 2.3 Ω for the different magnetic-core inductors, while the air core inductor is about 0.31 Ω. Sample P02 has only an inductance of 126 nH, but because of the small resistance, this sample reaches the highest quality factor of 43 at 30 MHz (Figure 6). The reference inductor Ref3 shows a strong increase of the resistance for higher frequencies, which leads to a disadvantage compared to the proposed inductors. Moreover,

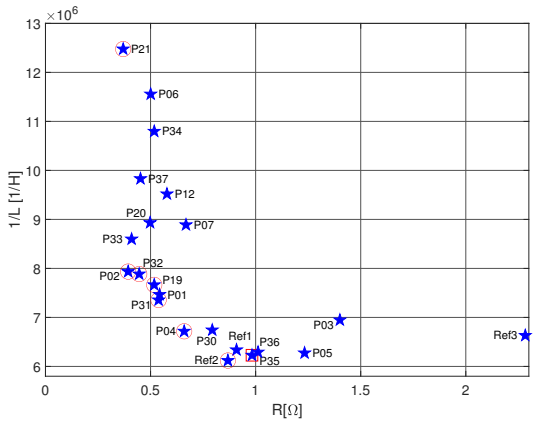

Figure 7 Pareto analysis at 20 MHz

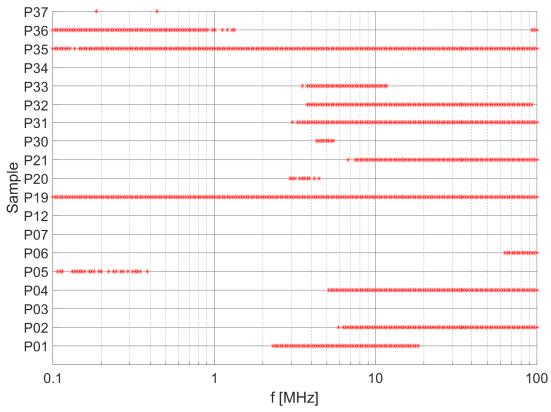

Figure 8 Pareto optimality over frequency

the Ref1 and Ref2 inductors have a slightly higher inductance and resistance, but compared to the other samples their quality factor is worse at 20 MHz.

For a better comparison, all samples were plotted with their resistance and inverse inductance in Figure 7 at 20 MHz. Now, a pareto analysis was executed to highlight all pareto-optimal samples (marked by a red circle). The other samples are dominated by at least one pareto-optimal sample, which has a higher inductance and a smaller resistance. Depending on the trade off between, whether a higher inductance or a smaller resistance is needed, one of the pareto-optimal (PO) samples should be picked. In addition, the three reference inductors are added to the plot, showing that Ref3 is dominated by sample P35. Ref1 has a better resistance but worse inductance than sample P35, therefore both would be part of the pareto front. Nevertheless, Ref2 is dominating Ref1 and sample P35, which makes Ref2 to one of the 7 pareto-optimal solutions for this frequency.

In Figure 8 the pareto-optimal samples for each frequency are marked. This shows that samples P03, P07, P12 and P34 are dominated by other samples over the whole frequency range, whereas sample P19 and P35 are always part of the pareto front. All in all, the plot clarifies which sample belongs to a possible solution at which frequency.

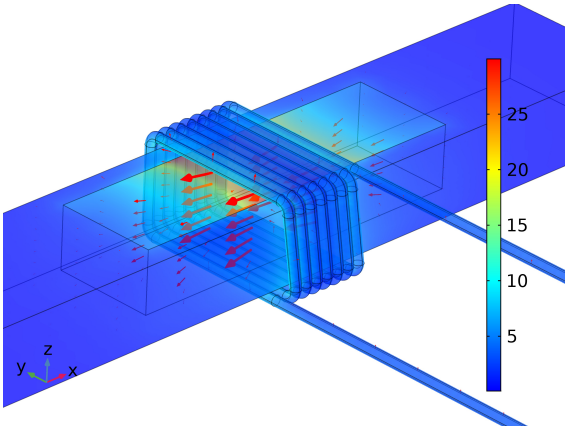

Figure 9 FEM, Magnetic flux density (in mT) at 20 MHz

4 FEM simulations

Here, Comsol Multiphysics is used as finite-element-method (FEM) simulation tool to investigate the electromagnetic behavior of these test samples in the frequency domain. First, the geometry of the sample was modeled; especially, the distance between the windings has a big impact on the magnetic flux density, respectively on the calculated inductance, therefore it was tried to adapt the model as close as possible to the real test setup. In the next step, standard material parameters are used for air, silicon and copper, but the main focus in this simulation work was a proper tuning of the powder based cores. Based on the measurement results of the VSM, the permeability of each sample was given and mostly the electrical conductivity has to be tuned. Due to the high frequencies, a detailed mesh grid for the wire is crucial to take the skin and proximity effect into account. Figure 9 shows the magnetic flux density at 20 MHz. The calculations are based on the magnetic field (mf) physics and the inductor is fed by a sinusoidal current of $I = 1\,\mathrm{A}$, whose frequency is swept from 100 kHz to 100 MHz. The maximal magnetic flux density is about $B = 30\,\mathrm{mT}$ in the simulation shown in Figure 9. Hence, the maximal magnetic field H is given by

$$H = \frac{B}{\mu_0 \mu_r} \approx 3500\,\mathrm{A/m}, \tag{2}$$

which is in the linear region of the hysteresis loop (Figure 4) for all 19 test samples except sample P21.

The evaluation of the inductance and resistance is done by measuring the complex impedance between both terminals of the inductor, which is given by

$$Z = R + j\omega L. \tag{3}$$

The inductance is calculated by dividing the imaginary part with the frequency and the resistance is given by the real part as follows

$$R = real\{Z\}, \qquad L = \frac{Im\{Z\}}{2\pi f}. \tag{4}$$

Assuming a permeability of $\mu = 6.8$, like sample P04, the effect of tuning the electrical conductivity σ of the powder

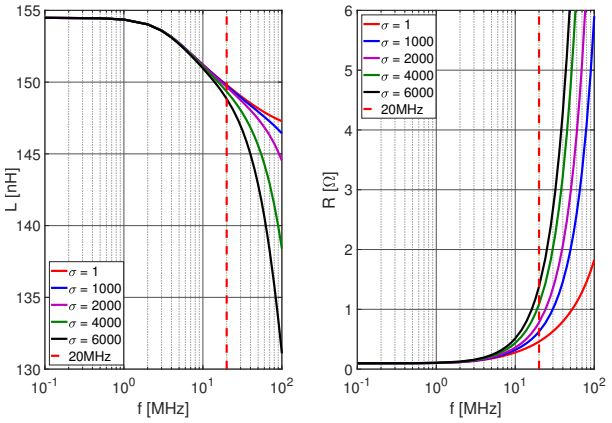

Figure 10 FEM simulation results (conductivity tuning)

based core is pointed out for the inductance and resistance in Figure 10.

These simulation results were compared with the measurement results from the impedance analyzer shown in the section before. Using an electrical conductivity of $\sigma = 1300\,\mathrm{S/m}$ and a permeability of $\mu = 6.8$, the simulation matches the measurements quite good. At 20 MHz the calculated inductance is about 148.80 nH and resistance is 668 mΩ, while the measured values are $L = 148.87\,\mathrm{nH}$ and $R = 660\,\mathrm{m\Omega}$. In Figure 5 the simulation results of sample P04 are plotted with a dashed line in the graph with the measured results, showing a quite accurate approximation. Therefore, a new powder with these parameters was added to the material library and is used for further designs and geometry optimizations. According to the fabrication possibilities, new designs with TSVs are in progress.

5 Conclusion

This paper presents a novel approach for the integration of inductances on silicon with a magnetic core for high switching frequency applications. These self-fabricated powder based cores were investigated on a scanning electron microscope and their hysteresis curves were plotted with a vibrating sample magnetometer. To obtain an inductor, these pieces were hand-wound with a copper wire to measure the inductance and resistance from 100 kHz to 100 MHz on an impedance analyzer. Based on these three measurements, 19 samples with different magnetic powders were compared. Furthermore, a FEM simulation model was set up and adapted to the measurement results by tuning the parameter of the magnetic powder. As a result, the accuracy of the simulation is proven and provides a basis for new designs and optimizations. The next steps will be the integration of a magnetic core inductor with TSVs on the same ceramic with new wide band gap power devices.

6 Literature

[1] D. Dinulovic, M. Shousha, M. Haug, A. Gerfer, M. Wens, and J. Thone, "On-chip high performance magnetics for point-of-load high-frequency DC-DC converters," in *2016 IEEE Applied Power Electronics Conference and Exposition (APEC)*, pp. 3097–3100, Mar. 2016.

[2] R. Meere, T. O'Donnell, H. J. Bergveld, N. Wang, and S. C. O'Mathuna, "Analysis of Microinductor Performance in a 20-100 MHz DC/DC Converter," *IEEE Transactions on Power Electronics*, vol. 24, pp. 2212–2218, Sept. 2009.

[3] N. Wang, J. Barry, J. Hannon, S. Kulkarni, R. Foley, K. McCarthy, K. Rodgers, F. Waldron, M. Barry, D. Casey, J. Rohan, J. O'Brian, M. Hegarty, A. Kelleher, S. Roy, and C. Ó. Mathúna, "High frequency DC-DC converter with co-packaged planar inductor and power IC," in *2013 IEEE 63rd Electronic Components and Technology Conference*, pp. 1946–1952, May 2013.

[4] N. Wang, J. Hannon, R. Foley, K. McCarthy, T. O'Donnell, K. Rodgers, F. Waldron, and C. Ó. Mathúna, "Integrated magnetics on silicon for power supply in package (PSiP) and power supply on chip (PwrSoC)," in *3rd Electronics System Integration Technology Conference ESTC*, pp. 1–6, Sept. 2010.

[5] M. Wang, J. Li, K. D. T. Ngo, and H. Xie, "A novel integrated power inductor in silicon substrate for ultra-compact power supplies," in *2010 Twenty-Fifth Annual IEEE Applied Power Electronics Conference and Exposition (APEC)*, pp. 2036–2041, Feb. 2010.

[6] N. Wang, T. O'Donnell, R. Meere, F. M. F. Rhen, S. Roy, and S. C. O'Mathuna, "Thin-Film-Integrated Power Inductor on Si and Its Performance in an 8-MHz Buck Converter," *IEEE Transactions on Magnetics*, vol. 44, pp. 4096–4099, Nov. 2008.

[7] P. R. Morrow, C. Park, H. W. Koertzen, and J. T. DiBene, "Design and Fabrication of On-Chip Coupled Inductors Integrated With Magnetic Material for Voltage Regulators," *IEEE Transactions on Magnetics*, vol. 47, pp. 1678–1686, June 2011.

[8] C. Ó. Mathúna, N. Wang, S. Kulkarni, and S. Roy, "Review of Integrated Magnetics for Power Supply on Chip (PwrSoC)," *IEEE Transactions on Power Electronics*, vol. 27, pp. 4799–4816, Nov. 2012.

[9] H. T. Le, I. Mizushima, Y. Nour, P. T. Tang, A. Knott, Z. Ouyang, F. Jensen, and A. Han, "Fabrication of 3D air-core MEMS inductors for very-high-frequency power conversions," *Microsystems & Nanoengineering*, vol. 4, p. 17082, Jan. 2018.

[10] X. Yu, J. Kim, F. Herrault, and M. G. Allen, "Silicon-embedded toroidal inductors with magnetic cores: Design methodology and experimental validation," in *2014 IEEE Applied Power Electronics Conference and Exposition - APEC 2014*, pp. 763–767, Mar. 2014.

[11] T. Lisec, T. Reimer, M. Knez, S. Chemnitz, A. V.

Schulz-Walsemann, and A. Kulkarni, "A Novel Fabrication Technique for MEMS Based on Agglomeration of Powder by ALD," *Journal of Microelectromechanical Systems*, vol. 26, pp. 1093–1098, Oct. 2017.

[12] T. Lisec, M. T. Bodduluri, A.-V. Schulz-Walsemann, L. Blohm, I. Pieper, S. Gu-Stoppel, F. Niekiel, F. Lofink, and B. Wagner, "Integrated High Power Micro Magnets for MEMS Sensors and Actuators," in *2019 20th International Conference on Solid-State Sensors, Actuators and Microsystems Eurosensors XXXIII (TRANSDUCERS EUROSENSORS XXXIII)*, pp. 1768–1771, June 2019.

[13] F. Steudel, T. Lisec, P. Nolte, U. Hofmann, T. Wantoch, F. Lofink, and S. Schweizer, "Pixelated phosphors for high-resolution and high-contrast white light sources: Erratum," *Optics Express*, vol. 27, p. 9097, Mar. 2019.

[14] F. Lofink, V. Tolstrup, T. Lisec, T. Reimer, A. Piorra, D. Meyners, E. Quandt, and B. Wagner, "Magnetically driven energy-harvester with monolithically integrated high-energy-density magnets," in *2017 19th International Conference on Solid-State Sensors, Actuators and Microsystems (TRANSDUCERS)*, pp. 351–354, June 2017.